Available online at www.sciencedirect.com
ScienceDirect
Free Radical Biology & Medicine 44 (2008) 682–691
www.elsevier.com/locate/freeradbiomed

Original Contribution

Assessment of wound-site redox environment and the significance of Rac2 in cutaneous healing

Navdeep Ojha [a], Sashwati Roy [a], Guanglong He [b], Sabyasachi Biswas [a], Murugesan Velayutham [b], Savita Khanna [a], Periannan Kuppusamy [b], Jay L. Zweier [b], Chandan K. Sen [a,*]

[a] *Laboratory of Molecular Medicine, Department of Surgery, Ohio State University Medical Center, Columbus, OH 43210, USA*
[b] *Department of Internal Medicine, Davis Heart and Lung Research Institute, Ohio State University Medical Center, Columbus, OH 43210, USA*

Received 30 September 2006; revised 25 October 2007; accepted 31 October 2007
Available online 17 November 2007

Abstract

We have previously reported that H_2O_2 is actively generated by cells at the wound site and that H_2O_2-driven redox signaling supports wound angiogenesis and healing. In this study, we have standardized a novel and effective electron paramagnetic resonance spectroscopy-based approach to assess the redox environment of the dermal wound site in vivo. Rac2 regulates inducible NADPH oxidase activation and other functional responses in neutrophils. Using Rac2-deficient mice we sought to investigate the significance of Rac2 in the wound-site redox environment and healing responses. Noninvasive measurements of metabolism of topically applied nitroxide ^{15}N-perdeuterated tempone in murine excisional dermal wounds demonstrated that the wound site is rich in oxidants, the levels of which peak 2 days postwounding in the inflammatory phase. Rac2-deficient mice had threefold lower production of superoxide compared to controls with similar wounds. In these mice, a lower wound-site superoxide level was associated with compromised wound closure. Immunostaining of wound edges harvested during the inflammatory phase showed that the numbers of phagocytic cells recruited to the wound site in Rac2-deficient and control mice were similar, but the amount of lipid peroxidation was significantly lower in Rac2-deficient mice, indicating compromised NADPH oxidase activity. Taken together, the findings of this study support that the wound site is rich in oxidants. Rac2 significantly contributes to oxidant production at the wound site and supports the healing process.

Keywords: Free radicals

Disrupted vasculature limits the supply of oxygen to the wound site. Compromised tissue oxygenation or wound hypoxia is viewed as a major factor that limits the healing process as well as wound disinfection [1]. The general consensus has been that, at the wound site, oxygen fuels tissue regeneration [2] and that oxygen-dependent respiratory burst is a primary mechanism to resist infection [3]. Recent work from our laboratory has developed a new paradigm supporting the notion that oxygen-derived reactive species at the wound site not only disinfect the wound but contribute directly to facilitating the healing process [4–7].

Wound healing commences with blood coagulation followed by infiltration of neutrophils and macrophages at the wound site to release reactive oxygen species (ROS) by oxygen-consuming respiratory burst. In 1999, the cloning of mox1 (later named Nox1) marked a major progression in categorically establishing the presence of distinct nicotinamide adenine dinucleotide phosphate (NADPH) oxidases in nonphagocytic cells [8]. Taken together, these observations indicate that the wound site has two clear sources of ROS: (i) transient delivery of larger amounts by respiratory burst of phagocytic cells and (ii) sustained delivery of lower amounts by enzymes of the Nox/Duox family present in cells such as fibroblasts, keratinocytes, and endothelial cells [5]. Recent studies show that, at low concentrations, ROS may serve as signaling messengers in the cell and regulate numerous signal transduction and gene expression processes [9]. Inducible ROS generated in some nonphagocytic cells are implicated in mitogenic signaling [10]. A direct role for NADPH oxidases and ROS in facilitating angiogenesis has been proven [4]. In line with these observations, we have previously reported that at the wound site, ROS

* Corresponding author. Fax: +1 614 247 7818.
E-mail address: chandan.sen@osumc.edu (C.K. Sen).

0891-5849/$ - see front matter © 2007 Elsevier Inc. All rights reserved.
doi:10.1016/j.freeradbiomed.2007.10.056

may promote wound angiogenesis by inducing VEGF expression in wound-related cells such as keratinocytes and macrophages [6]. In this study, we employed electron paramagnetic resonance (EPR) spectroscopy and spin trapping to assess the wound-site redox environment [11] and to develop an understanding of the role of Rac2-dependent oxidant production [12] in wound healing.

Materials and methods

Chemicals

^{15}N-PDT (4-oxo-2,2,6,6-tetramethylpiperidine-d_{16}-1-oxyl; CDN Isotopes, QC, Canada) was used as the nitroxide spin probe. At low concentration (<2 mM), ^{15}N-PDT produces a well-separated doublet EPR spectrum with a hyperfine-coupling constant of 2.2 mT. At higher concentrations, there is spin–spin broadening, which causes the two peaks to merge into one broad middle peak of lower amplitude. ^{15}N-PDT provides for enhanced sensitivity and a narrower line-width than non-isotope-enriched tempone. The nitroxide solution was prepared at 50 mM concentration in phosphate-buffered saline, subaliquoted, and kept frozen until use.

Copper,zinc-superoxide dismutase (SOD1) and catalase were obtained from Sigma Chemical Co. (St. Louis, MO, USA) and were of the purest grade available. Diethylenetriaminepentaacetic acid (DTPA) and 2,2,6,6-tetramethyl-1-piperidinyloxy (TEMPO) were obtained from Aldrich. Purified 5,5-dimethyl-1-pyrroline-*N*-oxide (DMPO) was obtained from Dojindo Laboratories (Kumamoto, Japan). Sources of other chemicals used are mentioned as they appear in the text.

Excisional dermal wound model

C57BL/6 mice between the ages of 8 and 10 weeks were used. Punch biopsy (3 mm) wounds were administered to the backs of mice in pairs (Fig. 1A) for L-band EPR experiments. The back of the mouse was shaved with standard animal hair clippers (No. 40 blade) and disinfected with betadine (Fisher, NJ, USA). Using microdissecting forceps (Roboz, Inc., MD, USA), the skin of the animal was lifted along the line as shown and a 3-mm dermal biopsy punch (Miltex, Inc., USA) was driven through the two folds of skin. Axially, the wounds were made just above the bridge of the back to avoid motion artifacts during EPR measurements. This resulted in two symmetrical full-thickness 3-mm-diameter wounds in the mouse without any underlying tissue damage. The separation between the two wounds was kept between 10 and 15 mm. A similar technique was used to create 8-mm punch wounds for X-band EPR spin trapping experiments.

For the wound-closure experiment, two 8×16-mm full-thickness excisional wounds [6] were made on the dorsal skin, equidistant from the midline and adjacent to the four limbs. Digital photographs of wounds in full view and in one plane were taken with a digital camera on specified days after wounding. Images were transferred to a computer and wound areas were calculated using the WoundMatrix software [4].

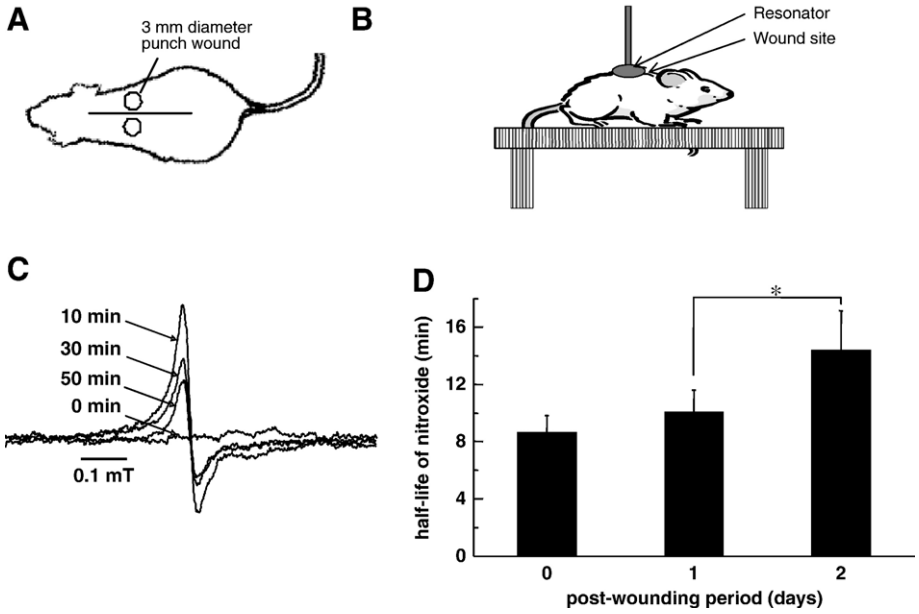

Fig. 1. Topical EPR spectroscopy of wounds. (A) Sketch of mouse with a pair of 3-mm full thickness dermal punch wounds (not drawn to scale). The distance between the wounds was 10–15 mm. These wounds were made above the bridge of the back so as to avoid motion artifacts caused by breathing while EPR spectroscopy measurements were being taken. (B) The mouse was anesthetized and placed on a height-adjustable table, which allows exact positioning of resonator above and around the wound site. (C) Time course of EPR spectra of ^{15}N-PDT after topical application to wound. The spectra were taken at the L-band using a surface resonator. A 6-μl solution of 50 mM PDT was applied to the wound site and spectral acquisitions were immediately started. Data acquisition parameters were as stated in the text. At the beginning of experiment the left and right peaks (only left peak shown here) were nonexistent. With time, these peaks appear and increase in intensity and then gradually decline. (D) Oxidant level at wound site increases 2 days after wounding. 3-mm punch biopsy wounds were made on the backs of C57BL/6 mice. 6 μl of 50 mM ^{15}N-PDT was topically applied to the wound and EPR spectra were immediately started. EPR spectra maxima of the left peak were used to generate decay curves, which were mathematically fitted, and half-life was calculated. Measurements were taken from the same wound on day 0, day 1, and day 2 after wounding. Data are shown as means±SD, $n=6$, *$p<0.05$.

EPR spectroscopy instrumentation for measurements in wound

EPR spectroscopy experiments were performed on an L-band spectrometer (Magnettech GmbH, Germany), which was set up for topical measurements on the skin of mice. A surface coil resonator of 10 mm diameter with automatic tuning and matching control was used. Mice were anesthetized with an intraperitoneal injection of ketamine (90 mg/kg) and xylazine (20 mg/kg) and placed in prone position between the poles of the magnet. The position of the animal was adjusted to place the surface resonator around the wound and in contact with the skin. After the system was tuned and matched, 6 μl of 50 mM PDT was topically applied to the wound site and EPR spectroscopy measurements were started. Measurements were taken for a minimum of 45 min or until the nitroxide EPR signal decayed completely, whichever was later. EPR spectroscopy parameters were chosen as follows: center field 44.4 mT, modulation amplitude 0.0135 mT, scan width 0.81 mT, scan time 20 s, microwave power 25 mW, time constant 0.1 s.

EPR spectra for spin trapping were recorded using quartz flat cells at room temperature with a Bruker ESP 300E spectrometer operating at X-band with 100-kHz modulation frequency and a TM_{110} cavity. DMPO (50 μl of 1 M) was topically applied to 2-day-old 8-mm punch biopsy wounds. After 10 min, the wound rinsate was collected from the wound cavity and diluted 20× in PBS containing DTPA, and its EPR spectra were recorded.

Direct H_2O_2 measurements

H_2O_2 levels in wound fluid were measured using a real-time electrochemical H_2O_2 measurement as described [13]. The Apollo 4000 system (WPI, Sarasota, FL, USA) was used for analysis. H_2O_2 was measured using the ISO-HPO-2 2.0-mm stainless steel sensor, with replaceable membrane sleeves and an internal refillable electrolyte. This electrode technology includes a H_2O_2-sensing element and separate reference electrode encased within a single Faraday-shielded probe design (WPI). Wound fluid was harvested from mice and was immediately used for direct H_2O_2 measurement as reported [4].

EPR data acquisition and analysis

EPR spectra were acquired and stored using the Analysis software (Magnettech GmbH.). The data were then converted into a special format that was read using custom-built software in our laboratory for visualization, analysis, and export of spectral parameters (e.g., intensity and line width) into Microsoft Excel, with which the final decay curves of the nitroxide were generated. Table Curve 2D software was used for mathematical modeling of nitroxide kinetics.

Quantitation of X-band EPR spectra was performed using custom-built software developed in our laboratory. Quantitation of the observed free radical signals was performed by computer simulation of the spectra and comparison of the double integral of the observed signal with that of a TEMPO standard (1 μM) measured under identical conditions [14].

Histology

Immunohistochemistry

Wounds developed with a 3-mm biopsy punch were collected on day 1 and day 2 using a 6-mm biopsy punch and embedded in OCT. Cryosections (10 μm) were cut and fixed in ice-cold acetone for 5 min. Peroxidase blocking was done by incubating the section with 0.3% H_2O_2 for 5 min before serum blocking with 10% goat serum. Primary antibody incubations were done as follows: anti-mouse neutrophil (Serotec), 1:100 for 1 h at room temperature; rabbit anti-HNE (Alexis), 1:500 for 1 h at room temperature; rat anti-mouse F4/80, 1:50 for 1 h at room temperature. Color was developed after incubating the section with the appropriate biotinylated secondary antibody (1:200) utilizing the ABC/DAB method (Vector) according to the manufacturer's instructions. Sections were counterstained with hematoxylin, dehydrated sequentially in alcohol with two changes of xylene, and mounted with permanent mount.

Immunofluorescence

Two-day-old 3-mm punch biopsy wounds, including the wound edge, were harvested with a 6-mm punch biopsy. Skin tissue was embedded in Optimal Cutting Temperature (OCT) compound and frozen. Sections (10 μm) were cut with a cryostat and fixed in acetone. Subsequently sections were blocked with 10% goat serum before being incubated with rabbit anti-hydroxynonenal (1:500; Alexis) and rat anti-mouse neutrophil (1:100; Serotec) together for 1 h at room temperature. After being washed, the sections were incubated in anti-mouse IgG conjugated to Alexa 488 and anti-rat IgG conjugated to Alexa 568 for 30 min at room temperature (both 1:100). Sections were counterstained with DAPI (1:10,000) and visualized under a Zeiss Axiovert 200M microscope.

For CD31 staining, cryosections were fixed in acetone and blocked with 10% BSA fraction V (Acros) for 30 min. Sections were then incubated with phycoerythrin-conjugated anti-mouse CD31 (1:100; eBiosciences) overnight at 4°C, counterstained with DAPI, and visualized as above.

Computer-assisted image analysis

A color-subtractive computer-assisted image analysis system was used to quantitatively label and calculate the immunostained area after staining and subsequent digital imaging [15]. We employed Adobe PhotoShop 6.0 with Image Processing Toolkit 5.0 (www.reindeergraphics.com) software for image analysis. This method, instead of performing positive color selection, serially removes all nonspecific color from the images using a sequential method of color background removal leaving behind only the positive stain on a white background. To remove sampling error caused by imaging only a part of the stained tissue, each

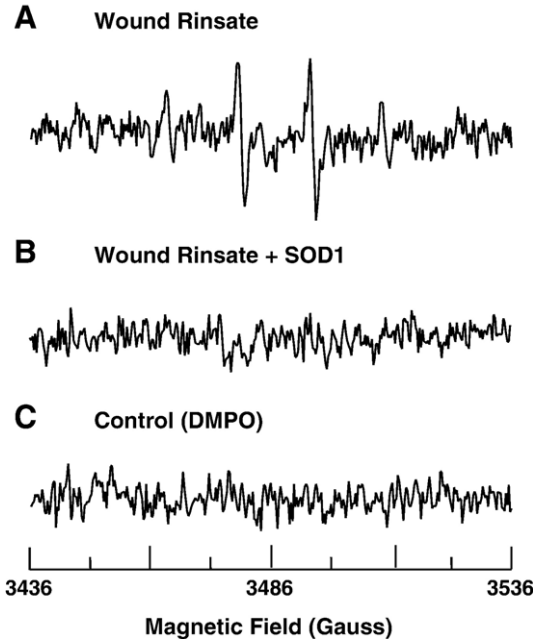

Fig. 2. Presence of superoxide at wound site. (A) The spectrum shows the presence of the spin adduct DMPO–·OH in the wound rinsate. 50 μl of 1 M DMPO was topically applied to 2-day-old 8-mm punch biopsy wounds. After 10 min the wound rinsate was collected from the wound cavity and diluted 20× in PBS containing DTPA, and its EPR spectrum was recorded. (B) 5 μl of SOD1 (300 μM) was topically applied to the wound 10 min before application of DMPO and subsequent collection of wound rinsate. Addition of SOD1 quenches the EPR signal, indicating that the source of signal is from superoxide. (C) Spectrum of DMPO in PBS. X-band EPR measurements were carried out using a quartz flat cell at room temperature. EPR instrument parameters used were as follows: microwave frequency 9.77 GHz, modulation frequency 100 kHz, modulation amplitude 1 G, microwave power 20 mW, number of scans 30, scan time 30 s, and time constant 81 ms.

tissue slide was imaged in three different areas at 20× magnification on a Zeiss microscope. Images were converted from the Zeiss ZVI format to standard JPEG format and loaded into Adobe PhotoShop for analysis.

All steps involved in image analysis were stored in a macro in Adobe PhotoShop. The macro was developed on an image selected at random from the images of the tissue sections. First, a copy of the layer containing the tissue section image was made. The color subtraction routine as described before [15] was modified as required for our images and executed on this new layer. Purple-pink stain of hematoxylin and other background color was colorimetrically removed and replaced with white, leaving behind a dark brown DAB color, which was the positive stain. The color subtraction process was continued until all nonspecific color was removed from the image. The color-subtraction layer was then duplicated and binary thresholding was performed on it. A threshold level of 252 was used. The thresholding routine converts all darker pixels above a selected threshold level to black and all pixels lighter than that to white. This results in a black and white image with positively stained areas in black on a white background. Feature measurement was then performed on this thresholded image to objectively calculate the area of stained tissue as a percentage of the complete image. The macro recording was then stopped, and the macro was saved. This macro is instrumental to generating immunostained areas from all sections automatically and efficiently without user bias.

Statistical analysis

All results are expressed as means±SD. The data were analyzed and compared using ANOVA and Student's *t* test

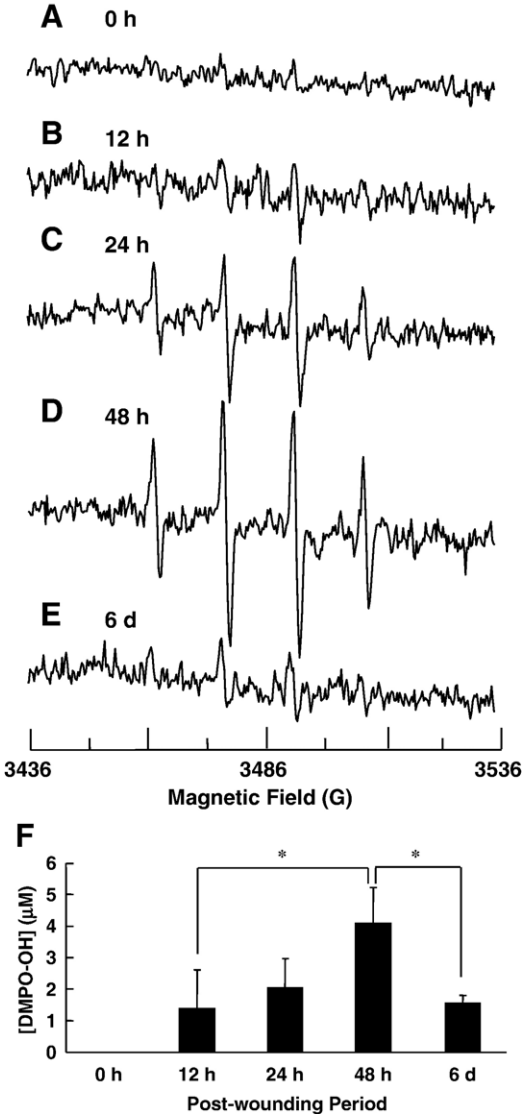

Fig. 3. Superoxide production at the wound site peaks 2 days after wounding as measured from DMPO spin adduct taken from the wound rinsate. EPR measurements were carried out as described before. X-band EPR spectra were recorded from wound rinsate collected at various time points as shown: (A) 0 h, (B) 12 h, (C) 24 h, (D) 48 h, and (E) 6 days. Clearly the maximum signal is obtained 48 h after wounding. (F) Quantitation of DMPO–·OH spin adduct formation in wound rinsate normalized to maximum intensity observed on day 2 after wounding. Quantitation was performed by computer simulation of the spectra and comparison of the double integral of the observed signal with that of a TEMPO standard (1 μM) measured under identical conditions. The increased production of superoxide correlates with the respiratory burst of inflammatory cells, which peaks at day 2 postwounding; $n=3$, $^*p<0.05$.

where appropriate for statistical significance. Differences between means at $p<0.05$ were considered significant.

Results

Nitroxide kinetics in wound

Using a noninvasive EPR-based technique we sought to quantify the oxidant concentration at the wound site in mice during the inflammatory phase, which lasts for about 2–3 days after wounding [16]. A nitroxide probe was topically applied to the open wound. Signal decay of the probe applied to the wound was monitored to generate a mathematical model to derive oxidant levels at the wound site. The nitroxide solution was topically applied to the dermal wounds (Fig. 1A) of mice and the resonator placed directly above and around the wound site (Fig. 1B). EPR spectroscopy measurements performed immediately after wounding were collected as a function of time and are shown in Fig. 1C. At the beginning, one broad peak was observed (0 min). This broad signal is attributed to electron spin exchange interaction of the nitroxide radicals in the concentrated solution at the surface of the skin [17]. With time, the broad central peak became narrower and weaker. In addition, another component with two sharp peaks (doublet) appeared, increased over the first 10 min, and then gradually declined because of reduction of nitroxide. Only the left peak is shown here in Fig. 1C, as the two side peaks were symmetrical. This component is a result of the diluted ^{15}N-PDT within the tissue, which gives rise to a doublet with hyperfine-coupling constant $a_N=2.2$ mT [18].

Oxidant levels at wound site peak 2 days after wounding

To estimate the level of oxidants at the wound site in the inflammatory phase of wound healing, the above-described

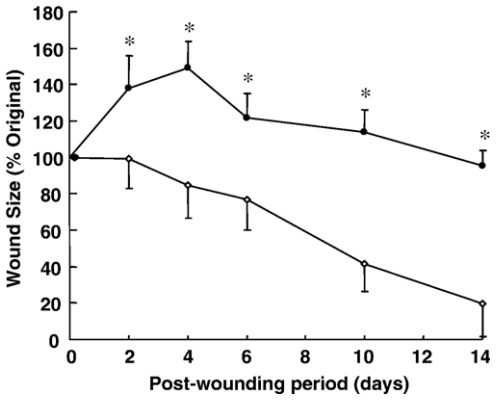

Fig. 4. Slow wound healing response of Rac2$^{-/-}$ animals. Two 8×16-mm full-thickness dermal wounds were created on the backs of Rac2$^{-/-}$ (filled circles) and wild-type (open diamonds) mice. Digital photographs of wounds in full view and in one plane were taken with a digital camera (Sony Mavica) on specified days after wounding. Wound areas were calculated using WoundMatrix software. *$p<0.05$; $n=4$ in each group.

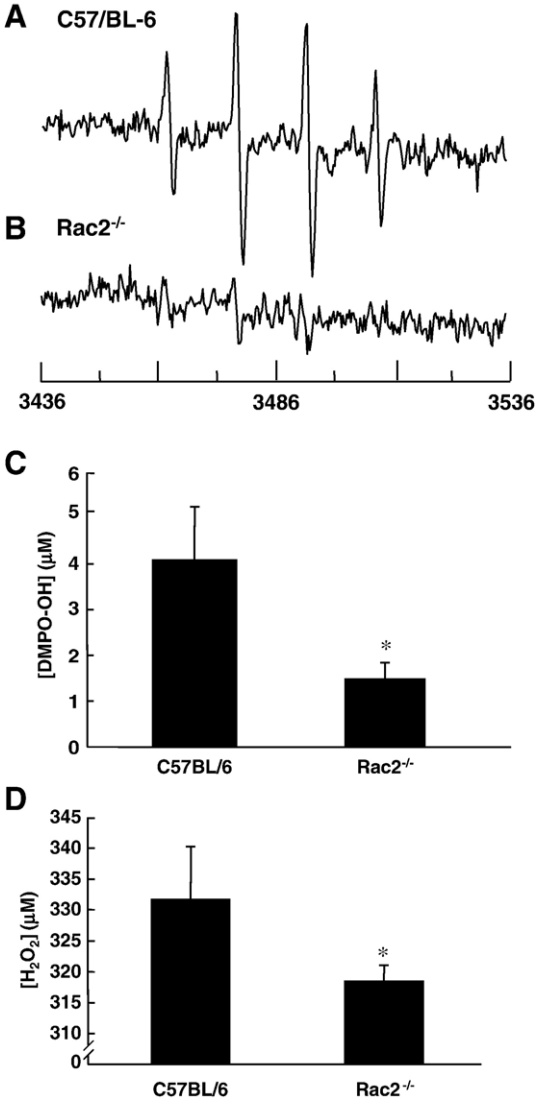

Fig. 5. Decreased superoxide production at wound site in Rac2$^{-/-}$ mouse corresponds to slow healing response of animals. (A and B) EPR measurements were done as described in the text at day 2 after wounding in wild-type and Rac2$^{-/-}$ mice. X-band EPR spectra of wound rinsate in PBS from (A) wild-type and (B) Rac2$^{-/-}$ mice are shown. (C) Quantitation of DMPO–$\dot{O}$H production in wild-type and Rac2$^{-/-}$ mice, indicating that a much lower amount of superoxide is produced in Rac2$^{-/-}$ mice given the compromised NADPH oxidase system in phagocytic cells. For this experiment, $n=3$ in each group. (D) H_2O_2 concentration in wound fluid. Hunt–Schilling cylinders were implanted in each of five 8-to 10-week-old C57BL/6 and Rac2$^{-/-}$ mice. On day 2, fluid was collected. 200 mM NaN_3 was added to inhibit peroxidase activity. To discern the H_2O_2-sensitive component of the signal detected in wound fluid 0.03 ml of the azide-free fluid was treated with 350 units of catalase. The catalase-sensitive component was interpreted as H_2O_2. Standard curve was generated using authentic H_2O_2 tested for UV absorbance. Data are shown as means±SD, $n=5$ in each group, *$p<0.05$.

EPR measurements were performed on day 0, day 1, and day 2 after wounding because the inflammatory phase in wounds lasts from day 0 to day 3 in mice [16]. Fig. 1D shows the change in half-life of nitroxide at the wound site with healing. It is known that the stability of a probe in a tissue characterizes the level of oxidants present at that

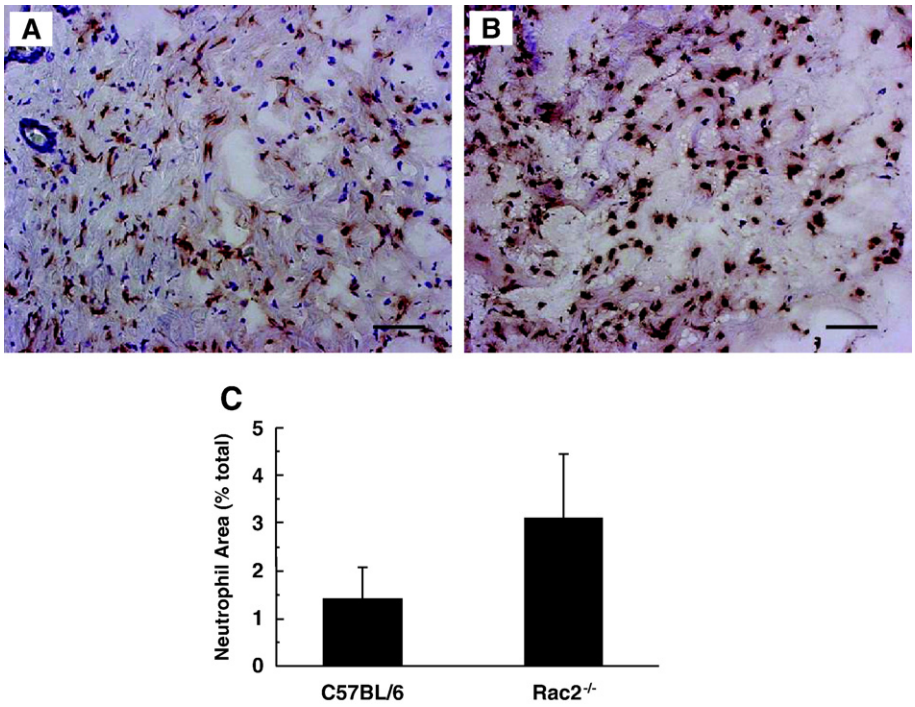

Fig. 6. Neutrophil recruitment to the wound site is increased in Rac2$^{-/-}$ mice. Neutrophil staining of (A) C57BL/6 mice and (B) Rac2$^{-/-}$ mice was performed on frozen sections of wound-edge tissue sampled 2 days after wounding. (C) Bar graph representing image analysis outcome. Three different regions from each wound were imaged on a microscope and analyzed with Adobe PhotoShop using a color-subtractive computer-assisted image analysis system. Rac2$^{-/-}$ mice show a trend toward higher recruitment of neutrophils to the wound site compared to wild type, possibly to compensate for the lower NADPH oxidase activity in the neutrophils. All images at 20× original magnification; scale bar, 50 μm; $n=4$ in each group.

location [18]. We observed that subsequent to wounding, the stability of the nitroxide probe at the wound site is higher (Fig. 1D). Thus, a higher concentration of oxidants was evident at the wound site on day 2 after wounding, which is the peak time for respiratory burst by the inflammatory cells [16].

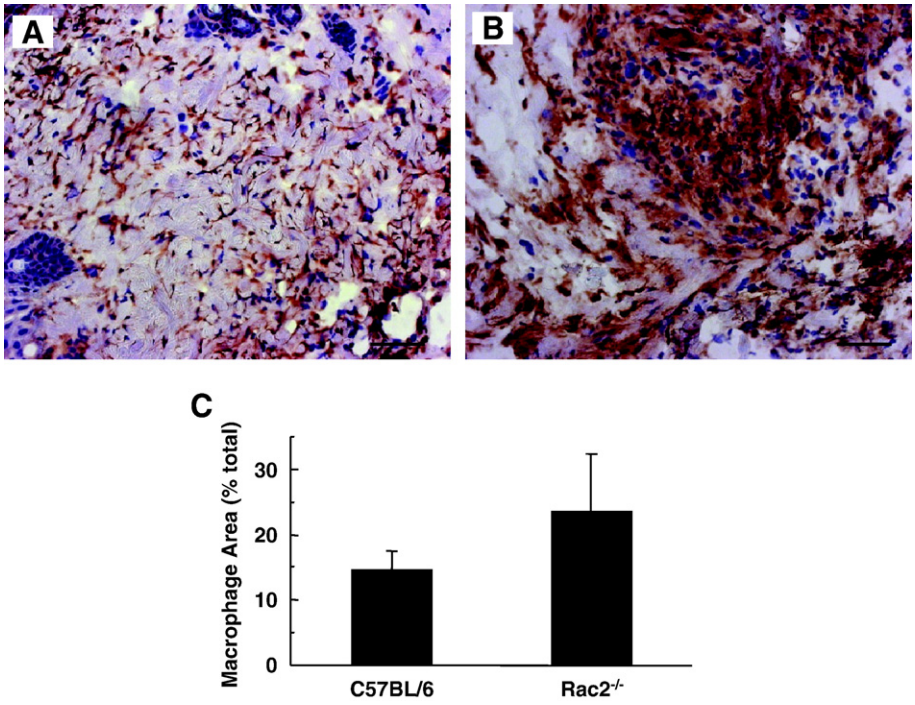

Fig. 7. Macrophage recruitment to the wound site is increased in Rac2$^{-/-}$ mice. F4/80 macrophage staining of (A) C57BL/6 mice and (B) Rac2$^{-/-}$ mice was performed on frozen sections of wound-edge tissue sampled 2 days after wounding. (C) Bar graph representing image analysis outcome. Rac2$^{-/-}$ shows a trend toward higher recruitment of macrophages to the wound site compared to wild type. All images at 20× original magnification; scale bar, 50 μm, $n=4$ in each group.

Spin trapping of superoxide radical with DMPO

After observing an oxidizing environment at the wound site with the nitroxide clearance approach, we employed DMPO as a spin trap to quantitate superoxide radical production in vivo. In the presence of DMPO, EPR analysis of wound rinsate in phosphate-buffered saline containing the metal ion chelator DTPA indicated formation of the spin trap radical adduct DMPO–˙OH. The spectrum in Fig. 2A, a 1:2:2:1 quartet that is not evident in the absence of wound rinsate (Fig. 2C), exhibited isotropic hyperfine splitting of $a_N = a_H = 1.49$ mT, characteristic of the hydroxyl radical adduct of DMPO, DMPO–˙OH. DMPO–˙OH can be formed by direct trapping of the hydroxyl radical by DMPO or as a product of decomposition of the superoxide radical adduct DMPO–OOH [19,20]. DMPO–OOH, with a half-life of 45 s in aqueous media, decomposes into a number of products, including DMPO–˙OH [21]. The abolishment of the DMPO–˙OH spectrum by the addition of SOD1 (Fig. 2B), further suggests that the DMPO–˙OH adduct is derived from superoxide. Thus, we concluded that the DMPO–˙OH spectrum noted at the wound site in our studies was caused by superoxide, the direct product of NADPH oxidases [5].

Next, we investigated the time course of superoxide generation at the wound site after wounding. Fig. 3 shows EPR spectra of wound rinsate collected at specific time points after wounding. We noted that superoxide production was at its maximum on day 2, when the inflammatory cells are actively engaged in respiratory burst activity. Quantitation of superoxide at the wound site is shown in Fig. 3F, in which the data are normalized to show relative concentrations. This corroborates our data on nitroxide decay (Fig. 1F) showing higher oxidant levels at the wound site 2 days after wounding.

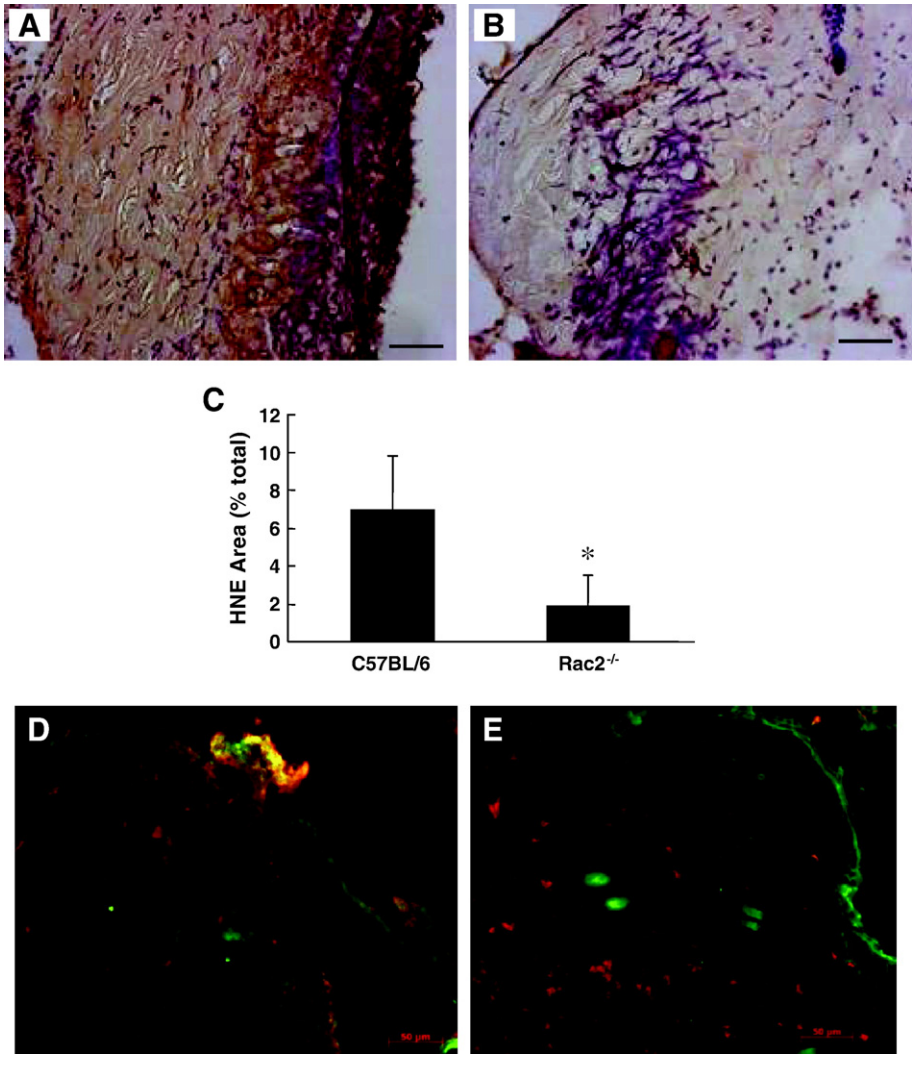

Fig. 8. Lower lipid peroxidation at the wound site in Rac2$^{-/-}$ mice. HNE staining was performed on OCT-fixed frozen sections of wound-edge tissue sampled 1 day after wounding. (A) Wild type. (B) Rac2$^{-/-}$ shows less lipid peroxidation indicative of lower (vs wild type) activity of inflammatory cells. (C) Bar graph represents image analysis outcome. (D and E) Double immunostaining was performed on OCT-fixed frozen sections of wound-edge tissue sampled 2 days after wounding. Wild type (D) shows higher level (vs Rac2$^{-/-}$ (E)) of colocalization of lipid peroxidation (green) and neutrophils (red), producing an orange-yellow hue all over the section, indicating that in Rac2$^{-/-}$ mice neutrophils infiltrate into the wound site but do not cause lipid peroxidation as they lack sufficient NADPH oxidase activity. All images at 20× original magnification; scale bar, 50 μm. Data are shown as means±SD, $n=4$ in each group, *$p<0.05$.

Impaired healing and compromised superoxide production in Rac2 knockout mice

NADPH oxidase deficiency impairs wound healing as is noted in chronic granulomatous disease [5]. Defects in the expression of any of the essential subunits of NADPH oxidase, e.g., Rac2, are expected to compromise respiratory burst-dependent oxidant production [22]. We noted that $Rac2^{-/-}$ mice suffer from significantly delayed wound closure (Fig. 4), indicating that Rac2-dependent NADPH oxidase activity is important in supporting wound healing. EPR spectra of wound rinsate collected from wild-type and $Rac2^{-/-}$ mice 2 days after wounding are shown in Figs. 5A and B, respectively. We chose this time point because the amount of superoxide production at the wound site in wild-type animals was found to be highest at day 2 (Figs. 1F and 3F). We observed a threefold decrease in superoxide production at the wound site in $Rac2^{-/-}$ mice compared to wild type (Fig. 5C). Quantitation of H_2O_2 in wound fluid using the electrochemical detection system showed significantly decreased peroxide concentration in wound fluid in $Rac2^{-/-}$ mice compared to matched wild type (Fig. 5D).

$Rac2^{-/-}$ mice: recruitment of phagocytic cells to wound site is not affected, but their function is impaired

When skin is wounded, the local tissue rapidly recruits inflammatory cells. Neutrophils reach the wound site in hours, followed by macrophages, which peak in day 2 after wounding [23]. We examined the wound-edge tissue from $Rac2^{-/-}$ mice and their corresponding wild-type mice. The number of neutrophils recruited to the wound-edge tissue on day 2 was imaged and scored using a color-subtractive computer-assisted image analysis method. Two days after wounding, $Rac2^{-/-}$ mice tended to recruit more neutrophils to the wound site but the difference was not statistically significant ($p=0.07$, Fig. 6). Consistent with the pattern noted for neutrophils, macrophage recruitment in $Rac2^{-/-}$ mice tended to be higher but the difference was not statistically significant ($p=0.11$, Fig. 7). Taking these observations together, it can be concluded that Rac2 deficiency did not compromise the ability of the mice to recruit inflammatory cells to the wound site.

At the wound site, inflammatory cells exhibit potent respiratory burst activity. 4-Hydroxy-2-nonenal (4-HNE) is a major product of endogenous lipid peroxidation which is found as a footprint in the aftermath of respiratory burst [24]. 4-HNE levels were clearly lower in the wound-edge tissue of $Rac2^{-/-}$ mice compared to that of wild-type controls (Figs. 8A–C). This observation is consistent with other results in this study demonstrating lower levels of reactive oxygen species in the wound of $Rac2^{-/-}$ mice. Employing a double immunostaining approach it was evident that in wound-edge tissue of wild-type mice neutrophils colocalize with 4-HNE stain, indicating active respiratory burst of the inflammatory cells (Fig. 8D). In the wound-edge tissue of $Rac2^{-/-}$ mice, however, neutrophils did not associate with strong 4-HNE stain, supporting other data in this study that indicate compromised respiratory burst activity in $Rac2^{-/-}$ mice (Fig. 8E).

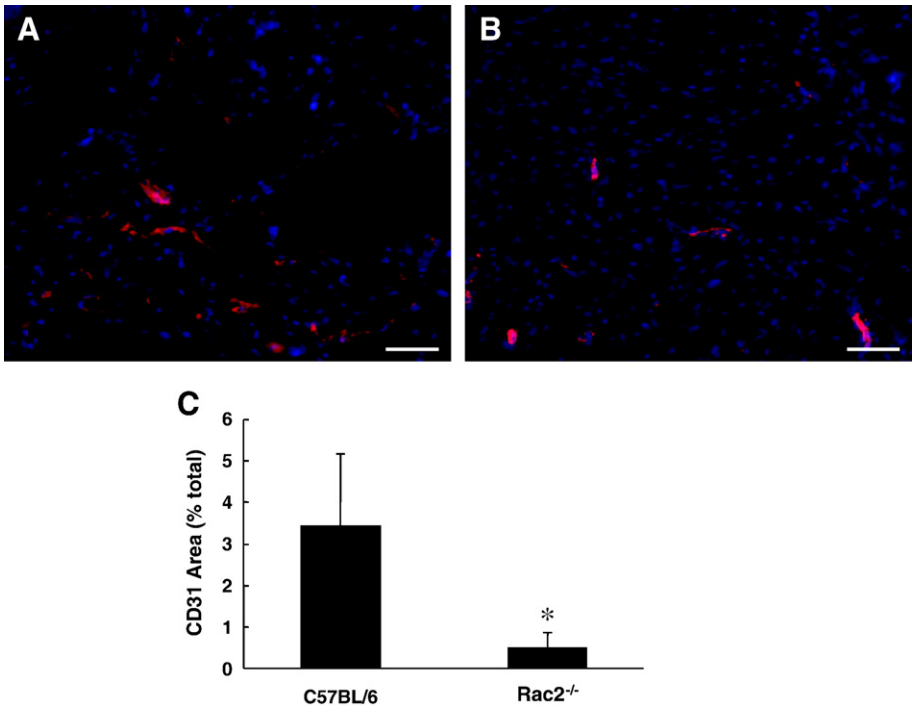

Fig. 9. Impaired angiogenesis in $Rac2^{-/-}$ mice. For estimation of vascularization, we performed immunohistochemical staining for CD31 (red) and DAPI (blue, nuclei) on cryosectioned wound tissue from (A) wild-type and (B) $Rac2^{-/-}$ mice sampled 8 days after wounding. (C) Bar graph representing image analysis outcome. The higher abundance of CD31 red stain in the section obtained from wild-type mice (left) demonstrates better vascularization and angiogenesis versus $Rac2^{-/-}$ (right). All images at 20× original magnification; scale bar, 50 μm; $n=4$ in each group.

Impaired angiogenesis in Rac2$^{-/-}$ mice

Rac2$^{-/-}$ mice suffer from significantly delayed wound closure (Fig. 4), indicating that Rac2 is an essential component for wound closure. CD31 is characteristic of endothelial cells. To study the role of Rac2 in angiogenesis we performed immunohistochemical staining for CD31 (red) and DAPI (blue, nuclei) on cryosectioned wound-edge tissue from wild-type and Rac2$^{-/-}$ mice sampled 8 days after wounding (Fig. 9). Compared to wild-type mice, the lower abundance of CD31 stain in the sections obtained from Rac2$^{-/-}$ mice (Fig. 9B) suggests impaired endothelial cell proliferation in mice deficient in Rac2.

Discussion

NADPH oxidase-dependent superoxide generation is highly active at the wound site [4]. The highest level of peroxide in bodily fluids is found in the wound [4]. At the wound sites, hydrogen peroxide drives wound angiogenesis [4] by inducing redox signaling [9]. Such redox-dependent mechanisms are compromised under conditions of NADPH oxidase deficiency. Thus, individuals with defective NADPH oxidase suffer from impaired healing, such as in chronic granulomatous disease [5]. On the other hand, approaches to facilitate NADPH oxidase activity at the wound site by Rac1 gene delivery promoted wound closure [6]. Rac GTPases, Rac1 and Rac2, are crucial regulators of NADPH oxidase function in eukaryotic cells [12]. In this work, using the nitroxyl spin probe ^{15}N-PDT, we observed that a healing wound is significantly rich in oxidants 2 days after wounding, which corresponds to the inflammatory phase. Lower stability of the probe corresponds to a more reductive state, and a higher stability corresponds to a more oxidative state of the wound tissue. This work presents the first evidence demonstrating the production of superoxide radicals at the wound site using a DMPO spin trapping technique. Basal superoxide production in the intact skin was below detection limits. Superoxide levels, however, sharply increased as a function of time. Superoxide levels were the highest at day 2 of healing, which corresponds to the peak time of respiratory burst of invading phagocytes [4]. We have previously developed instrumentation and methodology for noninvasive measurement and imaging of nitroxide spin labels in the skin of normal human volunteers [18]. This work represents a maiden effort to employ L-band and X-band EPR for quantitative measurement of redox status and spin trapping of superoxide radicals in full-thickness dermal wounds in mice.

Rac2 is a Rho GTPase that is expressed in cells of hematopoietic origin, including neutrophils and macrophages. Rac2 regulates reduced NADPH oxidase activation and other functional responses in neutrophils. Although not required for translocation of p47phox and p67phox, Rac2 is necessary for optimal activity of the assembled oxidase complex [22]. Mice deficient in hematopoietic-specific Rac2 exhibit agonist-specific defects in neutrophil functions, including superoxide production elicited by phorbol ester, fMLP, or IgG-coated particles, despite expression of the highly homologous Rac1 isoform. Although Rac2 is a relatively minor isoform in murine macrophages, it plays a nonoverlapping role with Rac1 to regulate host defense functions in this phagocyte lineage [22]. Consistent with these observations we noted that Rac2$^{-/-}$ mice suffer from impaired oxidant production at the wound site. EPR results showed that in Rac2-deficient mice oxidant production during the inflammatory phase was threefold lower than that in corresponding wild-type control mice. Lower levels of oxidants, under conditions of Rac2 deficiency, were associated with impaired wound closure. Rac2 deficiency has been reported in humans and is associated with poor wound healing [25]. In humans, Rac2 plays a critical and unique role to maintain normal neutrophil function [8].

Rac GTPases are believed to contribute to migration in leukocytes by transducing signals from cell surface receptors to the actin and microtubule cytoskeletons. Mammals have three closely related Rac isoforms, Rac1, Rac2, and Rac3, and it is widely assumed that cell migration requires the activity of these Rac GTPases. Rac1 and Rac2 have distinct roles in regulating cell morphology, migration, and invasion, but are not essential for macrophage migration or chemotaxis [26]. Consistent with this observation we noted that a lower level of oxidants at the wound site in Rac2$^{-/-}$ mice was not caused because of an impaired level of recruitment of phagocytic cells. The recruitment of both macrophages and neutrophils to the wound site was not impaired in Rac2$^{-/-}$ mice. Taken together, the findings of this study support that the wound site is rich in oxidants. Rac2 significantly contributes to oxidant production at the wound site and supports the healing process.

Acknowledgments

This work was supported by NIH-RO1 GM069589 and GM077185 to C.K.S.

References

[1] Gordillo, G. M.; Sen, C. K. Revisiting the essential role of oxygen in wound healing. *Am. J. Surg.* **186:**259–263; 2003.

[2] Kivisaari, J.; Vihersaari, T.; Renvall, S.; Niinikoski, J. Energy metabolism of experimental wounds at various oxygen environments. *Ann. Surg.* **181:**823–828; 1975.

[3] Greif, R.; Akca, O.; Horn, E. P.; Kurz, A.; Sessler, D. I. Supplemental perioperative oxygen to reduce the incidence of surgical-wound infection. Outcomes Research Group [see comment]. *N. Engl. J. Med.* **342:**161–167; 2000.

[4] Roy, S.; Khanna, S.; Nallu, K.; Hunt, T. K.; Sen, C. K. Dermal wound healing is subject to redox control. *Molec. Ther.* **13:**211–220; 2006.

[5] Sen, C. K. The general case for redox control of wound repair. *Wound Repair Regen.* **11:**431–438; 2003.

[6] Sen, C. K.; Khanna, S.; Babior, B. M.; Hunt, T. K.; Ellison, E. C.; Roy, S. Oxidant-induced vascular endothelial growth factor expression in human keratinocytes and cutaneous wound healing. *J. Biol. Chem.* **277:** 33284–33290; 2002.

[7] Sen, C. K.; Khanna, S.; Gordillo, G.; Bagchi, D.; Bagchi, M.; Roy, S. Oxygen, oxidants, and antioxidants in wound healing: an emerging paradigm. *Ann. N.Y. Acad. Sci.* **957:**239–249; 2002.

[8] Suh, Y. A.; Arnold, R. S.; Lassegue, B.; Shi, J.; Xu, X.; Sorescu, D.; Chung, A. B.; Griendling, K. K.; Lambeth, J. D. Cell transformation by the superoxide-generating oxidase Mox1. *Nature* **401:**79–82; 1999.

[9] Stone, J. R.; Yang, S. Hydrogen peroxide: a signaling messenger. *Antioxid. Redox Signal.* **8:**243–270; 2006.

[10] Irani, K.; Xia, Y.; Zweier, J. L.; Sollott, S. J.; Der, C. J.; Fearon, E. R.; Sundaresan, M.; Finkel, T.; Goldschmidt-Clermont, P. J. Mitogenic

signaling mediated by oxidants in Ras-transformed fibroblasts. *Science* **275:**1649–1652; 1997.

[11] Schafer, F. Q.; Buettner, G. R. Redox environment of the cell as viewed through the redox state of the glutathione disulfide/glutathione couple. *Free Radic. Biol. Med.* **30:**1191–1212; 2001.

[12] Hordijk, P. L. Regulation of NADPH oxidases: the role of Rac proteins. *Circ. Res.* **98:**453–462; 2006.

[13] Liu, X.; Zweier, J. L. A real-time electrochemical technique for measurement of cellular hydrogen peroxide generation and consumption: evaluation in human polymorphonuclear leukocytes. *Free Radic. Biol. Med.* **31:**894–901; 2001.

[14] Velayutham, M.; Villamena, F. A.; Navamal, M.; Fishbein, J. C.; Zweier, J. L. Glutathione-mediated formation of oxygen free radicals by the major metabolite of oltipraz. *Chem. Res. Toxicol.* **18:**970–975; 2005.

[15] Underwood, R. A.; Gibran, N. S.; Muffley, L. A.; Usui, M. L.; Olerud, J. E. Color subtractive-computer-assisted image analysis for quantification of cutaneous nerves in a diabetic mouse model. *J. Histochem. Cytochem.* **49:**1285–1291; 2001.

[16] Beanes, S. R.; Dang, C.; Soo, C.; Ting, K. Skin repair and scar formation: the central role of TGF. *Expert Rev. Mol. Med.* **2003:**1–22; 2003.

[17] Sachse, J. -H.; Marsh, D. Line intensities in spin-exchanged nitroxide ESR spectra. *J. Magn. Reson.* **68:**540–543; 1986.

[18] He, G.; Samouilov, A.; Kuppusamy, P.; Zweier, J. L. In vivo EPR imaging of the distribution and metabolism of nitroxide radicals in human skin. *J. Magn. Reson.* **148:**155–164; 2001.

[19] Finkelstein, E.; Rosen, G. M.; Rauckman, E. J.; Paxton, J. Spin trapping of superoxide. *Mol. Pharmacol.* **16:**676–685; 1979.

[20] Roubaud, V.; Sankarapandi, S.; Kuppusamy, P.; Tordo, P.; Zweier, J. L. Quantitative measurement of superoxide generation and oxygen consumption from leukocytes using electron paramagnetic resonance spectroscopy. *Anal. Biochem.* **257:**210–217; 1998.

[21] Rosen, G. M.; Pou, S.; Ramos, C. L.; Cohen, M. S.; Britigan, B. E. Free radicals and phagocytic cells. *FASEB J.* **9:**200–209; 1995.

[22] Yamauchi, A.; Kim, C.; Li, S.; Marchal, C. C.; Towe, J.; Atkinson, S. J.; Dinauer, M. C. Rac2-deficient murine macrophages have selective defects in superoxide production and phagocytosis of opsonized particles. *J. Immunol.* **173:**5971–5979; 2004.

[23] Witte, M. B.; Barbul, A. General principles of wound healing. *Surg. Clin. North Am.* **77:**509–528; 1997.

[24] Esterbauer, H.; Schaur, R. J.; Zollner, H. Chemistry and biochemistry of 4-hydroxynonenal, malonaldehyde and related aldehydes. *Free Radic. Biol. Med.* **11:**81–128; 1991.

[25] Ambruso, D. R.; Knall, C.; Abell, A. N.; Panepinto, J.; Kurkchubasche, A.; Thurman, G.; Gonzalez-Aller, C.; Hiester, A.; deBoer, M.; Harbeck, R. J.; Oyer, R.; Johnson, G. L.; Roos, D. Human neutrophil immunodeficiency syndrome is associated with an inhibitory Rac2 mutation. *Proc. Natl. Acad. Sci. U. S. A.* **97:**4654–4659; 2000.

[26] Wheeler, A. P.; Wells, C. M.; Smith, S. D.; Vega, F. M.; Henderson, R. B.; Tybulewicz, V. L.; Ridley, A. J. Rac1 and Rac2 regulate macrophage morphology but are not essential for migration. *J. Cell Sci.* **119:**2749–2757; 2006.